International Journal of Thermal Sciences 132 (2018) 486–497

Contents lists available at ScienceDirect

International Journal of Thermal Sciences

journal homepage: www.elsevier.com/locate/ijts

Detection of contact failures with the Markov chain Monte Carlo method by using integral transformed measurements

Luiz A.S. Abreu[a,b], Helcio R.B. Orlande[b,*], Marcelo J. Colaço[b], Jari Kaipio[c,d], Ville Kolehmainen[d], César C. Pacheco[b], Renato M. Cotta[b]

[a] Department of Mechanical Engineering and Energy, Polytechnic Institute/IPRJ, Rio de Janeiro State University – UERJ, Rua Bonfim 25, Nova Friburgo, RJ, 28625-570, Brazil

[b] Department of Mechanical Engineering, Politecnica/COPPE, Federal University of Rio de Janeiro – UFRJ, Cid. Universitária, Cx. Postal: 68503, Rio de Janeiro, RJ, 21941-972, Brazil

[c] Department of Mathematics, University of Auckland, Private Bag 92019, Auckland Mail Centre, Auckland, 1142, New Zealand

[d] Department of Applied Physics, University of Eastern Finland, P.O. Box 1627, 70211, Kuopio, Finland

A B S T R A C T

This work deals with the solution of an inverse heat conduction problem aiming at the detection of contact failures in layered composites through the estimation of the contact conductance between the layers. The spatially varying contact conductance is estimated using a Bayesian formulation of the problem and a Markov chain Monte Carlo method, with infrared camera measurements of the transient temperature field on the surface of the body. The inverse analysis is formulated using a data compression scheme, where the temperature measurements are integral transformed with respect to the spatial variable. The present approach is evaluated using synthetic measurements and experimental data from controlled laboratory experiments. It is shown that only few transformed modes of the data are required for solving the inverse problem, thus providing substantial reduction of the computational time in the Markov chain Monte Carlo method, as well as regularization of the ill-posed problem.

1. Introduction

The detection of internal failures in materials is a subject of extensive research due to its importance in several fields, for example, in structural health monitoring [1–14]. With the recent advancement and practical applications (e.g., in the aeronautic, space and petroleum industries) of composites consisting of layers of different materials, nondestructive and noninvasive methods for the detection of adhesion failures between the composite layers have been developed [2–15]. Heat transfer techniques can be found among these methods, by using qualitative [1,2,7,13,14] as well quantitative analyses based on the solutions of inverse problems [3–12].

In our previous works [3,4], the contact failures were detected through the estimation of the contact conductance between the layers of different materials from measurements of the transient temperature over the surface of the composite. The approach used in Refs. [3,4] was based on a Bayesian formulation of the inverse problem, with a total variation prior model for the unknowns and using the Markov chain Monte Carlo (MCMC) method for the inference of the Bayesian model. The computational complexity of MCMC with large dimensional problems is often prohibitive. Therefore, in this paper, we extend [3,4] to accommodate a data compression scheme. The temperatures measured with an infrared camera are spatially compressed through the integral transformation with eigenfunctions related to the actual physical problem. Only a few transformed modes are then used in the inverse analysis and the forward model is formulated directly in terms of the transformed (compressed) temperatures. A similar data compression approach was used in Refs. [16,17] for the estimation of spatially varying properties in a one-dimensional problem and is applied here with a two-dimensional transformation. The data compression applied in this work not only reduces the computational time required for the Markov chain Monte Carlo method, but also provides regularization for the inverse problem [18]. Conceptually, the integral transform data compression scheme falls within the broader class of orthogonal decomposition methods, such as POD – Proper Orthogonal Decomposition, Principal Component Analysis, Karhunen–Loeve decomposition and Truncated Singular Value Decomposition [19–25]. The accuracy of the proposed methodology is examined with simulated measurements, as well as with actual thermographic data obtained with controlled laboratory experiments [9], involving samples manufactured with

* Corresponding author.
E-mail address: helcio@mecanica.coppe.ufrj.br (H.R.B. Orlande).

https://doi.org/10.1016/j.ijthermalsci.2018.06.006
Received 2 July 2017; Received in revised form 27 March 2018; Accepted 4 June 2018
1290-0729/

Nomenclature

a,b,c	dimensions of the plate
$Bi_c(X,Y)$	dimensionless contact conductance
D	total number of measurements
$h_c(x,y)$	thermal contact conductance
k	thermal conductivity
k_{max}	number of transient measurements
$q(x,y,t)$	heat flux imposed on the top boundary
M	number of elements in the spatial grid
$\mathbf{P}$	vector of parameters
T	temperature
T_o	initial temperature in the medium
X,Y,Z	dimensionless spatial coordinates
Z_1	dimensionless position of the contact interface
$\mid \mathbf{A} \mid$	determinant of matrix ($\mathbf{A}$)

Greeks

α	thermal diffusivity
β	eigenvalue given by equation (6.a)
ϕ	eigenfunction given by equation (4.a)
γ	eigenvalue given by equation (6.b)
φ	eigenfunction given by equation (4.b)
θ	dimensionless estimated temperature
$\boldsymbol{\Theta}$	vector of estimated dimensionless temperatures
τ	dimensionless time
ψ	dimensionless measured temperature
$\boldsymbol{\Psi}$	vector of measured temperatures

Subscripts

1,2	plates 1 and 2, respectively
i,j	order of the eigenquantities in the X and Y directions, respectively
ref	reference values

Superscripts

*	dimensionless thermophysical properties and heat flux
$\bar{}$	transform in the X direction
$\sim$	transform in the Y direction

designed contact failures of different formats.

2. Physical problem and mathematical formulation

The physical problem considered here involves heat conduction through a plate with two layers, heated through its top surface by a heat flux q (x,y,t), as illustrated by Fig. 1. The bottom surface of the plate is thermally insulated and heat transfer is assumed negligible through its lateral surfaces. The plate is initially at a uniform temperature, T_o, and the physical properties of each layer are assumed homogeneous and not dependent on temperature. The length and width of the plate are a and b, respectively, while its thickness is denoted by c. A spatially distributed contact resistance between the two adjacent layers is modeled by a contact conductance h_c (x,y) [26]. For the inverse analysis, measurements of the temperature at the top (heated) surface of the plate, obtained with an infrared camera, are available.

The mathematical problem is written in dimensionless form by using the following variables:

$$\theta(X,Y,Z,\tau)=\frac{T(x,y,z,t)-T_o}{T_o} \qquad q^*(X,Y,\tau)=q(x,y,t)\frac{c}{k_{ref}T_o} \tag{1.a,b}$$

$$k^*=\frac{k}{k_{ref}} \qquad \alpha^*=\frac{\alpha}{\alpha_{ref}} \tag{1.c,d}$$

$$X=\frac{x}{c}$$
$$Y=\frac{y}{c}$$
$$Z=\frac{z}{c}$$
$$Z_1=\frac{c_1}{c}$$
$$A=\frac{a}{c}$$
$$B=\frac{b}{c} \tag{1.e-j}$$

$$\tau=\frac{\alpha_{ref}t}{c^2} \qquad Bi_c(X,Y)=\frac{h_c(x,y)c}{k_{ref}} \tag{1.k,l}$$

and we obtain:

$$\partial_\tau\theta_1(X,Y,\tau)=\alpha_1^*\nabla^2\theta_1 \text{ in } 0<X<A,\ 0<Y<B,\ 0<Z<Z_1,\ \text{for } \tau>0 \tag{2.a}$$

$$\partial_\tau\theta_2(X,Y,\tau)=\alpha_2^*\nabla^2\theta_2 \text{ in } 0<X<A,\ 0<Y<B,\ Z_1<Z<1,\ \text{for } \tau>0 \tag{2.b}$$

$$\partial_Z\theta_1=0 \text{ at } Z=0 \text{ in } 0<X<A,\ 0<Y<B \text{ and } \tau>0 \tag{2.c}$$

$$k_1^*\partial_Z\theta_1=k_2^*\partial_Z\theta_2 \text{ at } Z=Z_1 \text{ in } 0<X<A,\ 0<Y<B \text{ and } \tau>0 \tag{2.d}$$

$$k_1^*\partial_Z\theta_1=Bi_c(X,Y)[\theta_2-\theta_1] \text{ at } Z=Z_1 \text{ in } 0<X<A,\ 0<Y<B \text{ and } \tau>0 \tag{2.e}$$

$$k_2^*\partial_Z\theta_2=q^*(X,Y,\tau) \text{ at } Z=1 \text{ in } 0<X<A,\ 0<Y<B \text{ and } \tau>0 \tag{2.f}$$

$$\partial_X\theta_1=\partial_X\theta_2=0 \text{ at } X=0,\ 0<Y<B,\ 0<Z<1, \text{ and } \tau>0 \tag{2.g}$$

$$\partial_X\theta_1=\partial_X\theta_2=0 \text{ at } X=A,\ 0<Y<B,\ 0<Z<1, \text{ and } \tau>0 \tag{2.h}$$

$$\partial_Y\theta_1=\partial_Y\theta_2=0 \text{ at } Y=0,\ 0<X<A,\ 0<Z<1, \text{ and } \tau>0 \tag{2.i}$$

$$\partial_Y\theta_1=\partial_Y\theta_2=0 \text{ at } Y=B,\ 0<X<A,\ 0<Z<1, \text{ and } \tau>0 \tag{2.j}$$

$$\theta_1=\theta_2=0 \text{ at } \tau=0 \text{ in } 0 \text{ in } 0<X<A,\ 0<Y<B,\ 0<Z<1 \tag{2.k}$$

where the contact interface is located at $Z=Z_1$.

3. Forward problem

The forward (direct) problem associated with the formulation given by equation (2.a-k) involves the determination of the temperature fields $\theta_1(X,Y,Z,\tau)$ and $\theta_2(X,Y,Z,\tau)$. The direct problem corresponding to the transformed data is solved here by using a hybrid analytical-

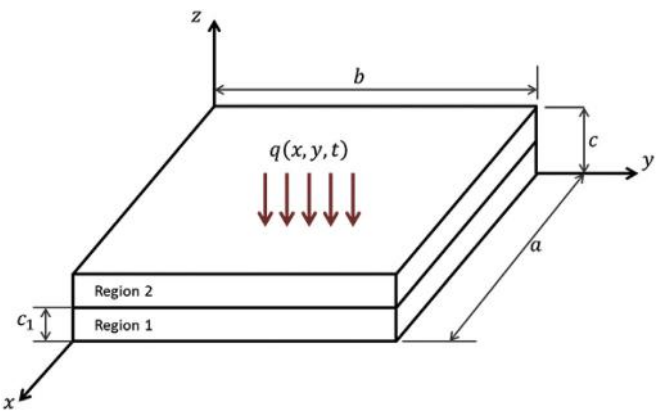

Fig. 1. Physical problem.

numerical approach, based on the Generalized Integral Transform Technique (GITT) [4,27–33] and finite differences [26,34].

Problem (2) is integral transformed along the X and Y directions by using the following transform – inversion formulae pair:

$$\text{Transform: } \widetilde{\bar{\theta}}_{1,2}(\beta_i, \gamma_j, Z, \tau) = \int_{X=0}^{A}\int_{Y=0}^{B} \bar{\phi}_i\, \bar{\varphi}_j\, \theta_{1,2}(X, Y, Z, \tau) dY\, dX \tag{3.a}$$

$$\text{Inversion formula: } \theta_{1,2}(X, Y, Z, \tau) = \sum_{i=0}^{\infty}\sum_{j=0}^{\infty} \bar{\phi}_i\, \bar{\varphi}_j\, \widetilde{\bar{\theta}}_{1,2}(\beta_i, \gamma_j, Z, \tau) \tag{3.b}$$

where the normalized eigenfunctions are obtained from Ref. [20]:

$$\bar{\phi}_i = \frac{\cos(X\beta_i)}{\sqrt{N_i}} \quad \bar{\varphi}_j = \frac{\cos(Y\gamma_j)}{\sqrt{N_j}} \text{ for } i = 0, \ldots, \infty \text{ and } j = 0, \ldots, \infty \tag{4.a,b}$$

with normalization integrals

$$N_i = A \quad \text{for } i = 0, \quad N_i = \frac{A}{2} \text{ for } i = 1, \ldots, \infty \tag{5.a}$$

$$N_j = B \quad \text{for } j = 0, \quad N_j = \frac{B}{2} \text{ for } j = 1, \ldots, \infty \tag{5.b}$$

and eigenvalues

$$\beta_i = \frac{i\,\pi}{A} \text{ for } i = 0, \ldots, \infty \tag{6.a}$$

$$\gamma_j = \frac{j\,\pi}{B} \text{ for } j = 0, \ldots, \infty \tag{6.b}$$

Hence, the following system of coupled equations for $i = 0, \ldots, \infty$ and $j = 0, \ldots, \infty$ results from the transformation of problem (2):

$$\frac{1}{\alpha_1^*}\frac{\partial \widetilde{\bar{\theta}}_1(\beta_i, \gamma_j, Z, \tau)}{\partial \tau} = \frac{\partial^2 \widetilde{\bar{\theta}}_1}{\partial Z^2} - (\beta_i^2 + \gamma_j^2)\widetilde{\bar{\theta}}_1 \text{ for } \tau > 0, \text{ in } 0 < Z < Z_1 \tag{7.a}$$

$$\frac{1}{\alpha_2^*}\frac{\partial \widetilde{\bar{\theta}}_2(\beta_i, \gamma_j, Z, \tau)}{\partial \tau} = \frac{\partial^2 \widetilde{\bar{\theta}}_2}{\partial Z^2} - (\beta_i^2 + \gamma_j^2)\widetilde{\bar{\theta}}_2 \text{ for } \tau > 0, \text{ in } Z_1 < Z < 1 \tag{7.b}$$

$$k_1^*\frac{\partial \widetilde{\bar{\theta}}_1}{\partial Z} = 0 \text{ at } Z = 0 \text{ and } \tau > 0 \tag{7.c}$$

$$k_2^*\frac{\partial \widetilde{\bar{\theta}}_2}{\partial Z} = \widetilde{\bar{d}}_{i,j} \text{ at } Z = Z_1 \text{ and } \tau > 0 \tag{7.d}$$

$$k_1^*\frac{\partial \widetilde{\bar{\theta}}_1}{\partial Z} = k_2^*\frac{\partial \widetilde{\bar{\theta}}_2}{\partial Z} \text{ at } Z = Z_1 \text{ and } \tau > 0 \tag{7.e}$$

$$k_1^*\frac{\partial \widetilde{\bar{\theta}}_{1,(i,j)}}{\partial Z} = \sum_{m=0}^{\infty}\sum_{u=0}^{\infty} A_{i,j,m,u}[\widetilde{\bar{\theta}}_{2,(m,u)} - \widetilde{\bar{\theta}}_{1,(m,u)}] \text{ at } Z = Z_1 \text{ and } \tau > 0 \tag{7.f}$$

$$\widetilde{\bar{\theta}}_1^* = \widetilde{\bar{\theta}}_2^* = 0 \text{ at } \tau = 0 \text{ in } 0 < Z < 1 \tag{7.g}$$

where

$$\widetilde{\bar{d}}_{i,j} = \int_{X=0}^{A}\int_{Y=0}^{B} q^*(X, Y, \tau)\bar{\phi}_i\, \bar{\varphi}_j\, dY\, dX \tag{8.a}$$

$$A_{i,j,m,u} = \int_{X=0}^{A}\int_{Y=0}^{B} \bar{\phi}_i\, \bar{\phi}_m\, \bar{\varphi}_j\, \bar{\varphi}_u\, Bi_c(X, Y) dY\, dX \tag{8.b}$$

The system of infinite coupled partial differential equation (7.a-g) for the transformed fields $\widetilde{\bar{\theta}}_1(\beta_i, \gamma_j, Z, \tau)$ and $\widetilde{\bar{\theta}}_2(\beta_i, \gamma_j, Z, \tau)$ was then discretized implicitly with finite differences along the Z direction [34]. The numerical solution was obtained by truncating the infinite system to a finite number of transform modes. The number of modes, as well as the finite difference grid size, was selected so that the computed fields $\theta_1(X, Y, Z, \tau)$ and $\theta_2(X, Y, Z, \tau)$ were within a user prescribed error tolerance. The double summations in equation (7.f) were rearranged in the form of a single summation, by using the two-dimensional eigenvalues $\beta_i^2 + \gamma_j^2$ in increasing order [33].

The numerical accuracy of the solution of the direct problem was verified in our previous works [3,4]. In this study, the inverse analysis in carried out with compressed data using integral transformation. In the following section, the solution of the direct problem in the transformed domain will be used for the definition of the likelihood function required for the solution of the inverse problem.

4. Inverse problem

The focus of this work is the detection of contact failures between layers 1 and 2 (see Fig. 1) by identifying the dimensionless contact conductance $Bi_c(X,Y)$. For perfect contact, $Bi_c(X,Y)$ is sufficiently large to characterize temperature continuity at the interface, while a contact failure is detected by values of the contact conductance that tend to zero. Simulated and real transient temperature measurements obtained with an infrared camera over the top surface $Z = 1$ will be used in an inverse analysis for the identification of $Bi_c(X,Y)$ (see below the section with the description of the experimental apparatus).

The inverse problem is solved through statistical inference on the posterior distribution of the model parameters, within the Bayesian framework of statistics [35–38]. In the Bayesian framework, all the unknown parameters are considered as random variables and modeled in terms of statistical distributions (priors) that represent their information and uncertainty before the experiment is performed. The priors are then combined with the information provided by the measurements taken during the experiment, which is also modelled in the form of a statistical distribution (likelihood), in order to obtain the posterior distribution of the parameters by using Bayes' theorem [35–38]:

$$\pi_{posterior}(\mathbf{P}) = \pi(\mathbf{P}|\mathbf{\Psi}) = \frac{\pi(\mathbf{P})\pi(\mathbf{\Psi}|\mathbf{P})}{\pi(\mathbf{\Psi})} \tag{9}$$

where $\pi_{posterior}(\mathbf{P})$ is the posterior probability density, $\pi(\mathbf{P})$ is the prior density, $\pi(\mathbf{\Psi}|\mathbf{P})$ is the likelihood function and $\pi(\mathbf{\Psi})$ is the marginal probability density of the measurements, which plays the role of a normalizing constant.

The posterior (9) is a probability density model of the inverse problem, defined on a high dimensional space. In this study, inference on the posterior model is carried out by sampling based on Markov chain Monte Carlo (MCMC) integration that is implemented through the Metropolis-Hastings' algorithm [35–46]. In the Metropolis-Hasting algorithm, a proposal distribution $p\ (\mathbf{P}^*,\mathbf{P}^{(t-1)})$, which is used to draw a new candidate $\mathbf{P}^*$ given the parameters in the current state $\mathbf{P}^{(t-1)}$ of the Markov chain, must be selected by the user. The proposal distribution can be, for example, random walk processes or independent moves based on the prior, but adaptive schemes are also available in the literature [35–38]. Once the proposal distribution has been selected, the Metropolis-Hastings algorithm can be described by the following steps [35–46]:

1. Sample a *Candidate Point* $\mathbf{P}^*$ from the proposal distribution $p\ (\mathbf{P}^*,\mathbf{P}^{(t-1)})$.
2. Calculate the acceptance factor:

$$R = \min\left[1\,,\ \frac{\pi(\mathbf{P}^*|\mathbf{\Psi})\, p(\mathbf{P}^{(t-1)}, \mathbf{P}^*)}{\pi(\mathbf{P}^{(t-1)}|\mathbf{\Psi})\, p(\mathbf{P}^*, \mathbf{P}^{(t-1)})}\right] \tag{10}$$

3. Generate a random value U that is uniformly distributed on (0,1).
4. If $U \le R$, set $\mathbf{P}^{(t)} = \mathbf{P}^*$. Otherwise, set $\mathbf{P}^{(t)} = \mathbf{P}^{(t-1)}$.
5. Return to step 1.

In this way, a sequence of random samples is generated to represent

the posterior distribution and inference on this distribution is obtained from inference on the samples $\{\mathbf{P}^{(1)}, \mathbf{P}^{(2)}, \ldots, \mathbf{P}^{(n)}\}$. We note that values of $\mathbf{P}^{(i)}$ must be ignored while the chain has not converged to equilibrium (the burn-in period).

In this work the dimensionless contact conductance $Bi_c(X,Y)$ is modeled as piecewise constant in each pixel of a grid with center points (X_I,Y_J), where $X_I = I\Delta X$, $Y_J = J\Delta Y$, $I = 1, \ldots, I_f$, $J = 1, \ldots, J_f$, and with grid spacing given by $\Delta X = A/I_f$ and $\Delta Y = B/J_f$. The total number of estimated points, which cover the spatial domain $0 < X < A$ and $0 < Y < B$, is then $M = I_f\, J_f$. The applied heat flux is analogously modeled as piecewise constant on a similar discretization of the top surface. Hence, the vector of unknown parameters for the inverse analysis is given by:

$$\mathrm{P}^T = [Bi_{c1},\ Bi_{c2},\ \ldots, Bi_{cM},\ q_1^*,\ q_2^*,\ \ldots, q_M^*,\ \alpha_1^*,\ \alpha_2^*,\ k_1^*,\ k_2^*] \tag{11}$$

The priors used for the parameters will be discussed below. The vector containing the measured temperatures is written as:

$$\mathbf{\Psi}^T = (\vec{\psi}_1\ ,\ \vec{\psi}_2\ ,\ \ldots\ ,\ \vec{\psi}_{k_{\max}}) \tag{12.a}$$

where $\vec{\psi}_k$ contains the measured temperatures of each of the M grid elements at time t_k, $k = 1, \ldots, k_{max}$, that is,

$$\vec{\psi}_k = (\psi_{k1}\ ,\ \psi_{k2}\ ,\ \ldots\ ,\ \psi_{kM}) \text{ for } k = 1,\ldots, k_{max} \tag{12.b}$$

so that we have $D = M\, k_{max}$ measurements in total.

Temperature measurements obtained with an infrared camera have errors that can be modeled as Gaussian, with zero mean and constant standard deviation σ [18,44]. Therefore, the *likelihood function* can be expressed as [3,4,35–46]:

$$\pi(\mathbf{\Psi}|\mathbf{P}) = (2\pi\sigma^2)^{-D/2} \exp\left\{-\frac{1}{2}\frac{[\mathbf{\Psi}-\Theta(\mathbf{P})]^T[\mathbf{\Psi}-\Theta(\mathbf{P})]}{\sigma^2}\right\} \tag{13}$$

where $\mathbf{\Theta}(\mathbf{P})$ is the solution of the direct (forward) problem, given by equation (2.a-k) with vector $\mathbf{P}$ given by equation (11).

The solution of the direct problem, $\mathbf{\Theta}(\mathbf{P})$, needs to be computed for all states of the Markov chain, at each position and time that a measurement is available. Typically, the number of states required for the Markov chain to generate samples that appropriately represent the posterior distribution is very large. Therefore, if the computational time for the solution of the direct problem is large, the application of the Markov chain Monte Carlo method for the solution of the inverse problem (acquiring an adequate number of samples with the MCMC chain) might not be feasible for general purpose computers. The use of fast reduced mathematical models for the solution of the direct problem in the inverse analysis, instead of the complete model that accurately represents the physics of the problem, can be formally treated within the Bayesian framework by modeling the approximation errors as Gaussian random variables and modifying the likelihood, such as in the Approximation Error Model [35,47–52]. Sampling techniques like the Delayed Acceptance Metropolis-Hastings algorithm [53,54] have also been developed in order to expedite the application of Markov chain Monte Carlo methods with the use of reduced models. Besides the three-dimensional nature of the heat conduction problem in this work, the large computational times for the solution of the present inverse problem result from the number of measurements made available by the infrared camera, which can provide experimental data with high spatial resolution and high frequency. Therefore, instead of applying model reduction and using either the Approximation Error Model or the Delayed Acceptance Metropolis-Hastings algorithm, a data compression approach is applied here in order to reduce the computational work needed for the calculation of the likelihood function. We note, however, that with a drastic model reduction, the estimates might turn out to be misleading (in the sense of predicted posterior covariance). In such a case, the Approximation Error Models might be called for.

Data compression in this work is performed by transforming the experimental data (temperatures at each pixel recorded by the infrared camera) with the same integral transform that is used in the forward model, equation (3.a), that is,

$$\widetilde{\overline{\psi}}(\beta_i, \gamma_j, \tau) = \int_{X=0}^{A}\int_{Y=0}^{B} \overline{\phi}_i\, \overline{\phi}_j\, \psi(X, Y, \tau)\, dY\, dX \tag{14.a}$$

Such as for $\widetilde{\overline{\theta}}_1(\beta_i, \gamma_j, Z, \tau)$ and $\widetilde{\overline{\theta}}_2(\beta_i, \gamma_j, Z, \tau)$, the transformed measured data, $\widetilde{\overline{\psi}}(\beta_i, \gamma_j, \tau)$, were ordered with increasing eigenvalue $\beta_i^2 + \gamma_j^2$. The number of transformed modes was selected as the same used for the solution of problem (7. a-g), by also taking into account that the inversion of (14. a) with

$$\psi(X, Y, \tau) = \sum_{i=0}^{\infty}\sum_{j=0}^{\infty} \overline{\phi}_i\, \overline{\phi}_j\, \widetilde{\overline{\psi}}(\beta_i, \gamma_j, \tau) \tag{14.b}$$

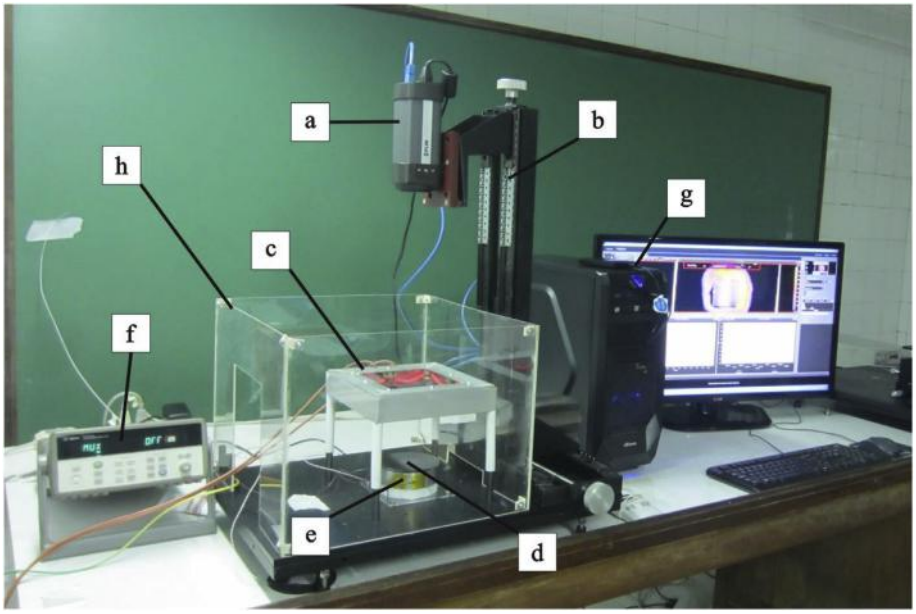

Fig. 2. Experimental apparatus: (a) Infrared camera, (b) Camera holder, (c) Radiating heater, (d) Sample, (e) Sample holder, (f) Data acquisition system, (g) Microcomputer for data acquisition, (h) Plexiglass dome.

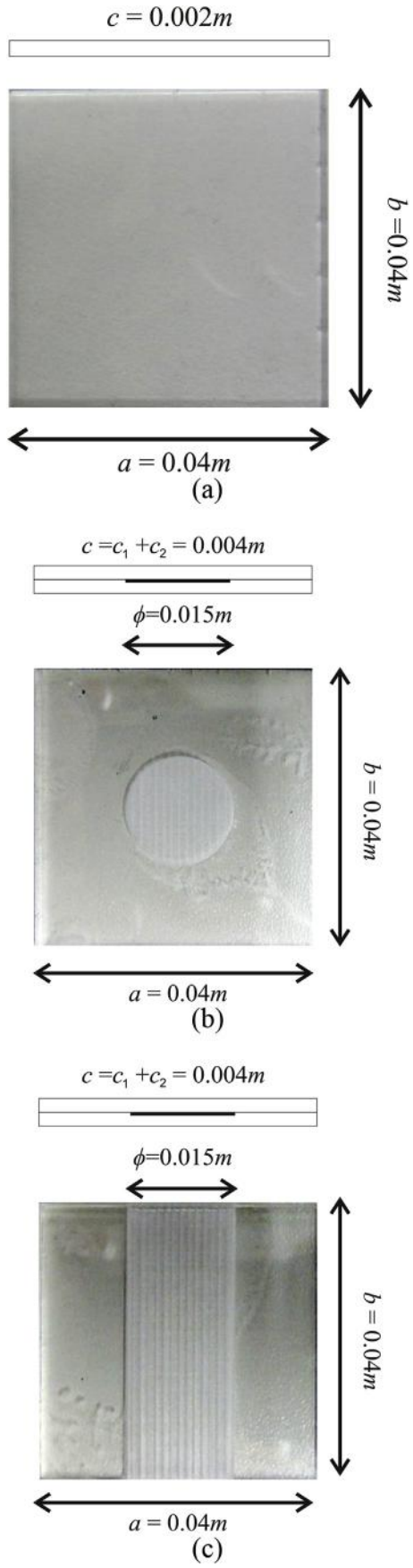

Fig. 3. Manufactured plates: (a) Without contact failures, (b) With a circular contact failure, (c) With a longitudinal contact failure.

must be represented up to desired accuracy by the truncated series. An estimate for the number of eigenmodes can be computed based on the related eigenvalues for any desired accuracy.

Since the transformation given by equation (14.a) is linear, and using the fact that the standard deviation of the measurements is constant, the covariances of the transformed measurements $\widetilde{\overline{\psi}}(\beta_i, \gamma_j, \tau)$ are then given by:

$$\widetilde{\overline{\sigma}}^2(\beta_i, \gamma_j, \tau) = \sigma^2 \int_{X=0}^{A} \int_{Y=0}^{B} \overline{\phi}_i \overline{\phi}_j \, dY \, dX \tag{15}$$

With the transformed measurements obtained with equation (14.a), $\widetilde{\overline{\Psi}}$, and with the transformed estimated temperatures obtained with the solution of the forward problem given by equation (7.a-g) at $Z = 1$ and each time that a measurement is available, $\widetilde{\overline{\Theta}}(\mathbf{P})$, the likelihood function can be rewritten in the transformed domain as

$$\pi(\widetilde{\overline{\Psi}}|\mathbf{P}) = (2\pi)^{-\widetilde{D}/2} |\widetilde{\overline{W}}|^{-1/2} \exp\left\{-\frac{1}{2}[\widetilde{\overline{\Psi}} - \widetilde{\overline{\Theta}}(\mathbf{P})]^T \widetilde{\overline{W}}^{-1} [\widetilde{\overline{\Psi}} - \widetilde{\overline{\Theta}}(\mathbf{P})]\right\} \tag{16}$$

where $\widetilde{\overline{W}}$ is the covariance matrix of $\widetilde{\overline{\Psi}}$, with elements given by equation (15).

Vectors $\widetilde{\overline{\Psi}}$ and $\widetilde{\overline{\Theta}}(\mathbf{P})$ are computed at a limited number of transformed modes, $\widetilde{D}$, much smaller than the actual number of measurements, D, thus resulting in substantial reduction of computational times required for the solution of the inverse problem, as will be apparent below. The integrals required for the transformation of the measurements and their covariances were respectively computed numerically (with the interpolation of $\psi(X, Y, \tau)$ by cubic splines) and analytically.

5. Experiments

An experimental apparatus was constructed in order to validate the approach for the detection of contact failures described above (see Fig. 2). The experimental apparatus is composed of [9]: (a) Infrared camera FLIR A325sc with 320 × 240pixels and measurement frequency of 9 Hz; (b) Camera holder; (c) Radiating heater; (d) Sample; (e) Sample holder; (f) Data acquisition system (Agilent 34970-A); (g) Microcomputer for data acquisition; and (h) Plexiglass dome to reduce flow over the sample from the air conditioning system. The whole system was assembled over a table used for laser experiments, in order to obtain precise positions that are maintained throughout the different experiments. The radiating heater consisted of a bare electrical resistance fixed with ceramic insulators inside an aluminum groove. The internal and external surfaces of the lower part of the groove were coated with graphite (Graphit 33, Kontact Chemie), in order to increase their absorptivity and emissivity, respectively, aiming at a uniform flux over the sample. The samples where the detection of contact failures was sought were located in a support made of plexiglas, styrofoam and aluminum. This support was attached to the table, at the center of the square heater, so that the sample orientation was maintained from one experiment to another. The distances from the sample to the heater and to the camera were kept as 100 mm and 400 mm, respectively. The plexiglas plate that maintained the sample position and orientation also served as thermal insulation for its lateral surfaces, while the styrofoam block served as thermal insulation for the sample lower surface.

In order to validate the inverse problem approach of this work, samples containing known controlled contact failures were manufactured by using square plates made of polymethyl methacrylate. The plate dimensions were $a = b = 0.04$ m and $c_1 = c_2 = 0.002$ m. Grooves with different shapes and depths ranging from 100 μm to 150 μm (measured with a 3D Digital Microscope 3D Hirox model KH-8700) were micro-machined in one of the plates. After cleaning, the plate containing the groove was carefully attached to another plate without any grooves by using chloroform. Hence, the contact between the plates was ideally perfect, except at the location of the machined groove.

Samples containing a circular and a longitudinal contact failure are

presented by Fig. 3. This figure also shows a sample made of one single plate, without any grooves, which was prepared for validation of the method and for the estimation of the heat flux imposed by the radiating heater. The samples were all coated with a very thin graphite layer (Graphit 33, Kontact Chemie). This coating served to increase and make more uniform the imposed heat flux over the sample surface, as well as to increase and control emissivity in the infrared range for accurate measurements with the infrared camera.

Temperatures measured with the infrared camera were recorded with the software FLIR ResearchIR™ at a rate of 9 frames per second. Before the experiments were started, the equilibrium temperatures were recorded for 10 s in order to compute the standard deviation of the measurements, which was of 0.03 °C.

6. Results and discussions

Results obtained with simulated measurements, as well as with actual measurements in the experiment described above, are reported and discussed in this section. For all cases, the prior for the dimensionless contact conductance was taken as a uniform improper distribution in the form

$$\pi(Bi_c(X, Y)) = \begin{cases} 1 & , \quad Bi_c(X, Y) \geq 0 \\ 0 & , \quad Bi_c(X, Y) < 0 \end{cases} \tag{17}$$

where, the non-negativity constraint for the contact conductance was imposed. An upper bound for the prior of $Bi_c(X, Y)$ was not imposed because $Bi_c(X, Y) \rightarrow \infty$ in the perfect contact. On the other hand, from the practical point of view, values of $Bi_c(X,Y)$ larger than 10 already characterize perfect contact for the cases examined below, because the temperature difference across the interface becomes negligible, as given by equation (2.e).

6.1. Verification with simulated measurements

Simulated measurements were used for the verification of the inverse problem procedure, based on measurements in the transformed domain and the non-informative prior given by equation (17). Two plates with dimensions $a = b = 0.10$ m and thicknesses of 0.005 m ($c = 0.01$ m), representative of titanium ($k = 21.9$ W/mK and $\alpha = 9.32 \times 10^{-6}$ m^2/s) and epoxy with graphite fibers ($k = 0.87$ W/mK and $\alpha = 0.66 \times 10^{-6}$ m^2/s) were used for this verification test [4]. A heat flux of 25 kW/m^2 was imposed uniformly over the titanium plate. The surfaces of the plates were allowed to exchange heat by convection with the surrounding environment, with heat transfer coefficients taken as 10 and 100 W/m^{2}K at the bottom and top surfaces of the plate, respectively, such as in Ref. [4]. The initial temperature was assumed as 25 °C. The thermophysical properties and the initial and boundary condition parameters were supposed known for this verification with simulated measurements. The frequency of the simulated measurements was 10 Hz and the duration of the simulated experiment was taken as 10s. The simulated contact failures were given in the form of two squares with sides of 0.005 m (see Fig. 4a). The contact conductance was discretized on a mesh with 31 × 31 pixels. The simulated measurements contained additive Gaussian random noise with zero mean and standard-deviation of 0.05 °C, therefore larger than those of the actual measurements (see previous section).

The dimensionless contact conductance estimated with simulated measurements and with a symmetrical proposal density [4], by using 50 transformed modes, is presented in Fig. 4b. A comparison of Fig. 4a and 4b reveals that the contact failures were accurately detected with the proposed approach. Furthermore, Fig. 4b shows that the estimated contact conductance was stable with respect to the measurement errors and did not exhibit oscillations, despite the fact that its prior is non-informative. Regularization was provided by the selection of the number of transformed modes, as will be further discussed below when actual measurements are used for the solution of the inverse problem.

For this test-case, 96100 temperature measurements were available (experiment with duration of 10s, measurements with a frequency of 10 Hz on a 31 × 31 grid). On the other hand, 50 modes were used for the solution of the inverse problem with the likelihood function in the transformed domain (see equation (16)), thus resulting on a data compression of 94.7%. Despite such large data compression through the integral transformation of the measurements, the spatial information provided by the transformed modes was still sufficient to recover two small contact failures, such as given by Fig. 4a,b.

The reduction of the computation time required for the solution of the inverse problem was substantial, when the likelihood function in the transformed domain was used. The solution of the inverse problem using MCMC took 6.3 days with the regular likelihood given by equation (13), while the MCMC run using the likelihood in the transformed domain took less than 2 h, resulting on a speedup of 79. For both cases, the solutions were obtained with 30000 states in the Markov chains and by neglecting the first 10000 states (burn-in period). Computational times refer to a FORTRAN code running on an Intel Core I7-2600 with 3.4 GHz clock and 16 Gb of RAM memory.

6.2. Validation with actual measurements

The thermophysical properties of the polymethyl methacrylate, used for manufacturing the plates for the controlled experiments, as described in the previous section, were measured by using the Flash method (NETZSCH LFA-441). The measured thermal diffusivity and

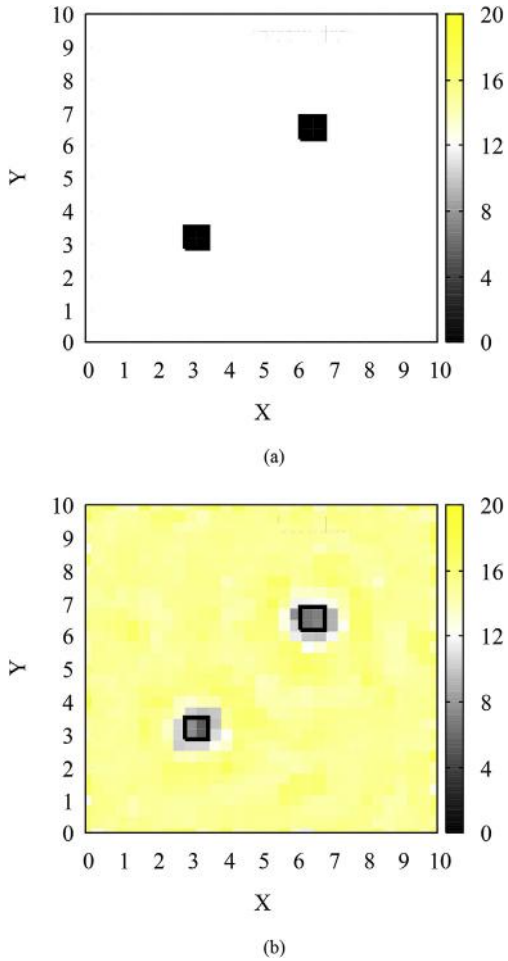

Fig. 4. (a) Exact dimensionless contact conductance used to generate the simulated measurements, (b) Dimensionless contact conductance estimated with simulated measurements.

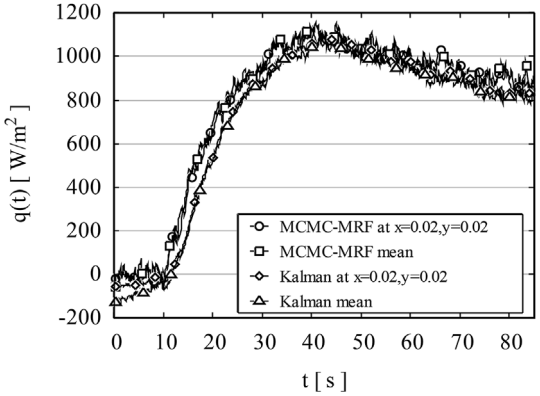

Fig. 5. Estimated heat flux.

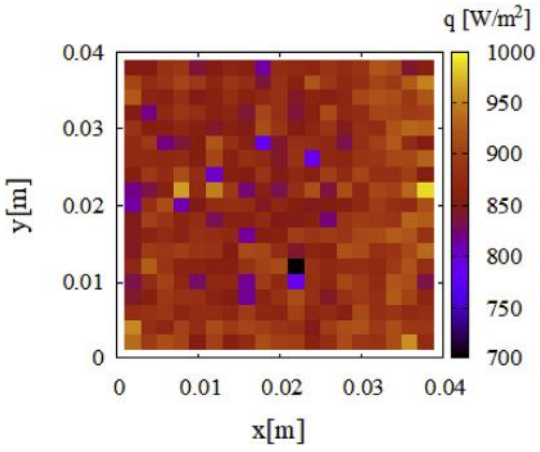

Fig. 6. Estimated heat flux with Kalman filter at $t = 85$ s.

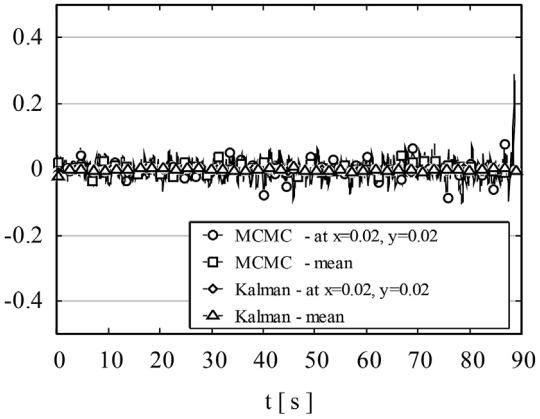

Fig. 7. Temperature residuals for the estimation of the imposed heat flux.

thermal conductivity were 1.31×10^{-7} m^{2}s^{-1} and 0.22 Wm^{-1}K^{-1}, respectively, which are in excellent agreement with the values reported in the literature [55]. For the estimation procedures presented below, uncertainties in these parameters were taken into account through their priors, which were modeled as Gaussian distributions centered at these measured values, with standard deviations set to 10% of the measured values from the Flash experiment, of 1.31×10^{-8} m^{2}s^{-1} and 0.022 Wm^{-1}K^{-1}, respectively.

Before addressing the identification of the contact failures of the actual samples, the heat flux imposed by the radiating heater was estimated by inverse analyses within the Bayesian framework, as well. Two different techniques were used for the estimation of the heat flux

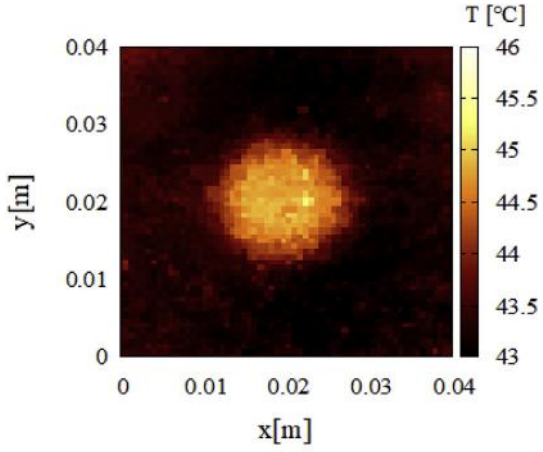

(a)

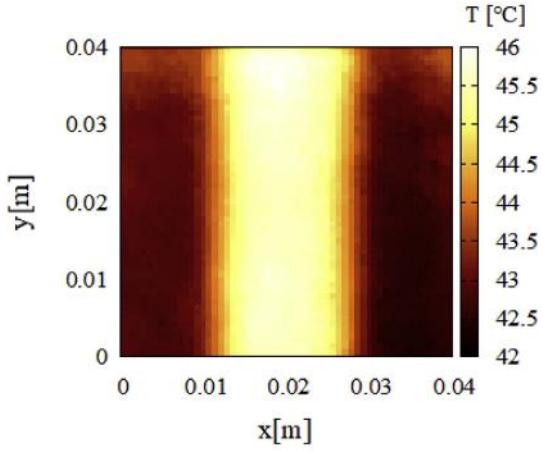

(b)

Fig. 8. Measured temperatures at $t = 90$ s: (a) Plate with circular contact failure.

in an inverse heat conduction problem in the plate without contact failures (see Fig. 3a), namely: Markov chain Monte Carlo (MCMC) method [41] and Kalman filter [51,52]. Temperature measurements taken with the infrared camera were used for the estimation of the imposed heat flux in an experiment with duration of 90 s. The Markov chain Monte Carlo method was applied for a one-dimensional problem, where the imposed heat flux only varies in time, but not over the surface of the plate [41]. The motivation for estimating a transient heat flux in a one-dimensional problem was the experimental result that the temperature was practically uniform at the surface of the plate without contact failures. The transient temperatures recorded at different pixels were individually used for the estimation with the MCMC method. Moreover, the MCMC method was applied with the transient spatial mean temperature over the surface of the plate. The prior used for the heat flux was a Gaussian Markov Random field, such as in Ref. [41]. As a validation of the heat flux estimated with the one-dimensional model using MCMC, the Kalman filter was also applied, such as in Refs. [51,52]. For the estimation of the heat flux with the Kalman filter, the more general case of a spatially varying transient function, $q(x,y,t)$, was considered with all the transient measurements taken over the sample surface. Details of the procedures used for the estimation of the imposed heat flux are avoided here but can be readily found in Refs. [41,51,52].

Fig. 5 compares different estimations obtained for the imposed heat flux, including: (i) the transient heat flux estimated by using MCMC with the measurements of one single pixel located at $x = y = 0.02$ m; (ii) the transient heat flux estimated by using MCMC with the spatial

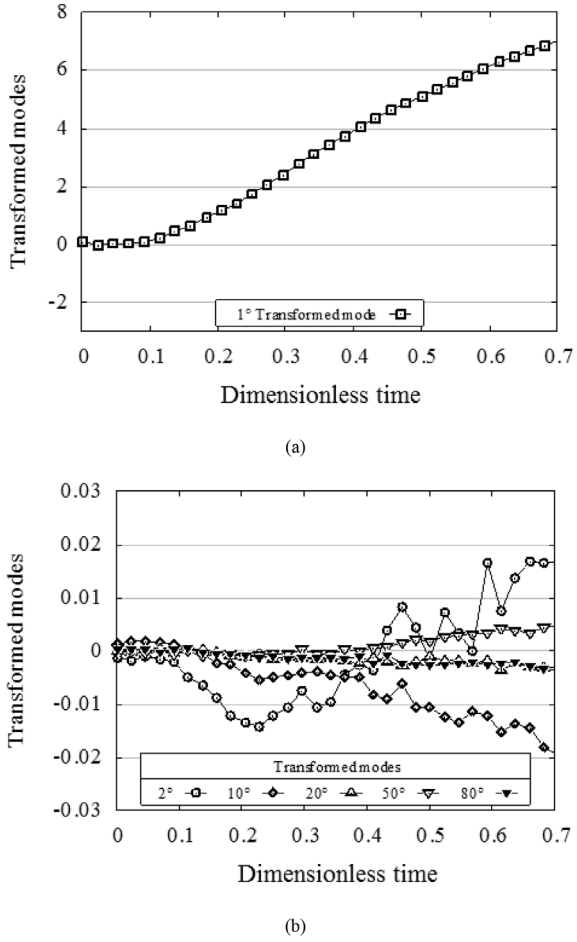

Fig. 9. Transformed dimensionless measured temperature modes for the plate with circular failure: (a) First mode, (b) Other selected modes.

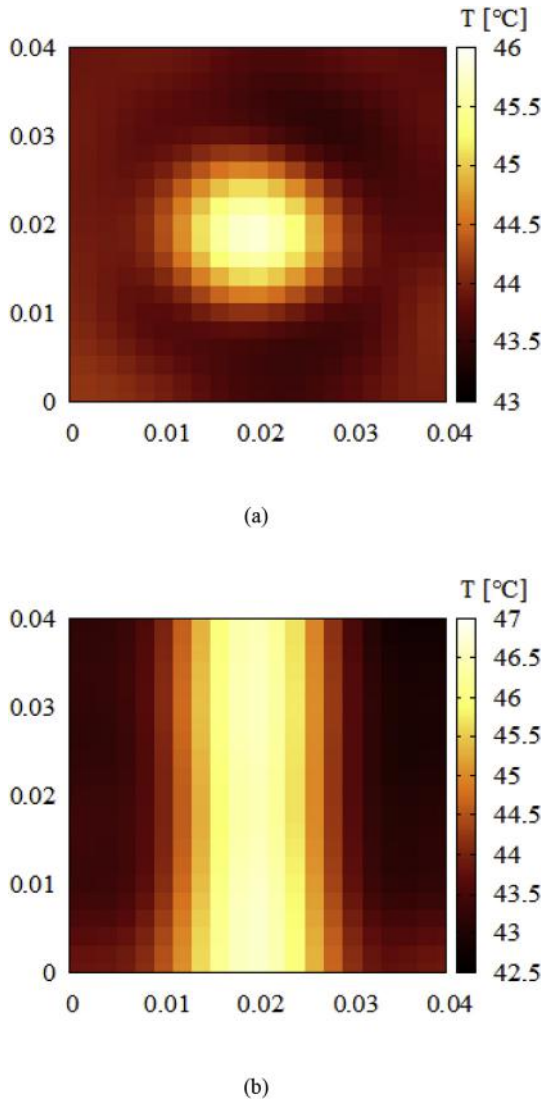

Fig. 10. Measured temperatures recovered after transformation with 50 modes at $t = 90$ s:
(a) Plate with circular contact failure, (b) Plate with longitudinal contact failure.

mean of the transient measured temperatures; (iii) the local transient heat flux q (x,y,t) estimated with the Kalman filter at $x = y = 0.02$ m; (iv) the mean of the local heat fluxes estimated with the Kalman filter at all pixels. We note in Fig. 5 that the heat fluxes estimated with the different approaches are in excellent agreement, indicating that the radiating heater provides a practically uniform flux over the sample. Negative heat flux values are observed in Fig. 5 with the Kalman filter estimates, because this is a sequential technique. Actually, the heat flux was null during the pre-heating period, as correctly estimated with MCMC which is a whole-domain technique. Fig. 6 shows the local heat fluxes at $t = 85$ s estimated with the Kalman filter, which practically has a uniform distribution over the plate, with few oscillations that can be attributed to the ill-posed character of the problem. The temperature residuals (differences between measurements and temperatures calculated with the estimated heat fluxes) are presented in Fig. 7; the residuals are quite small and uncorrelated, indicating the accuracy of the estimated heat fluxes and that there are no mismatches between the physical problem and the mathematical formulations used for the estimation of the imposed heat flux.

For the estimation of the contact conductance $Bi_c(X,Y)$ presented hereafter, the prior for the heat flux, $[q_1^*,\ q_2^*,\ ...,q_M^*]$, was given in the form of Gaussian distributions, with means and covariances obtained from the Kalman filter estimation described above. In addition, the proposal density was given by the following nonsymmetrical random walk process

$$\mathbf{P}^* = \mathbf{P}^{(t-1)} + \omega(\delta 1 + \mathbf{N}) \tag{18}$$

where 1 is a vector with all elements equal to one and $\mathbf{N}$ is a vector with elements taken from a Gaussian distribution with zero mean and unitary standard deviation. This nonsymmetrical proposal density was used in order to avoid a large rejection of candidates $\mathbf{P}^*$, specially in the regions of contact failure where the expected value of $Bi_c(X,Y)$ is zero, since this function needs to satisfy the non-negativity constraint (see equation (17)). For the results presented below, which were obtained with this proposal density, the acceptance ratio of candidate states was around 27%.

The measured temperatures at the final time (duration of the experiment) $t = 90$ s are presented by Fig. 8a,b, for the plates with the circular and the longitudinal contact failures, respectively (see Fig. 3b,c). The temperature measurements are available on a grid with 60×60 pixels over the top surface of the plate. Fig. 8a,b shows that, in the present experiments, the contact failures could be identified to some extent by a qualitative analysis of the surface temperature variation. However, for the estimation of the contact conductance such qualitative information was not taken into account, in order to challenge the method for the quantitative identification of the contact failures with a non-informative prior. Furthermore, to be able to make the decision about the existence of a contact failure, one needs to know the posterior means together with the associated variances, which are readily

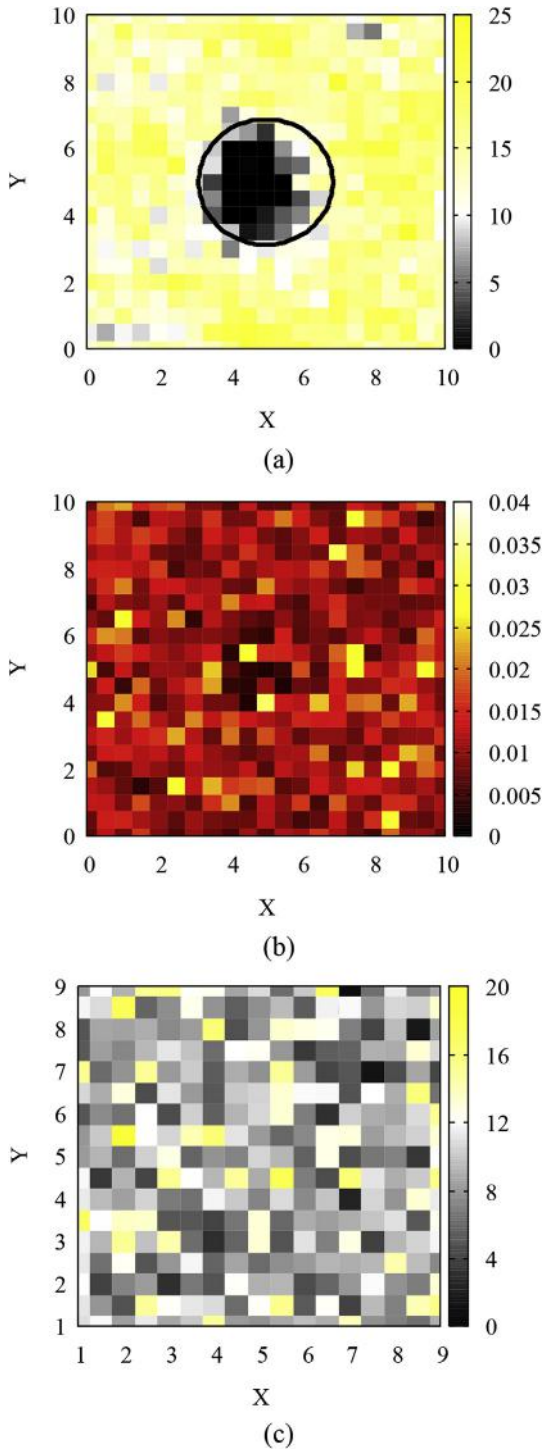

Fig. 11. Dimensionless contact conductance for the plate with circular failure: (a) Estimated means obtained with 50 modes, (b) Estimated standard deviations obtained with 50 modes (c) Estimated means obtained with 200 modes.

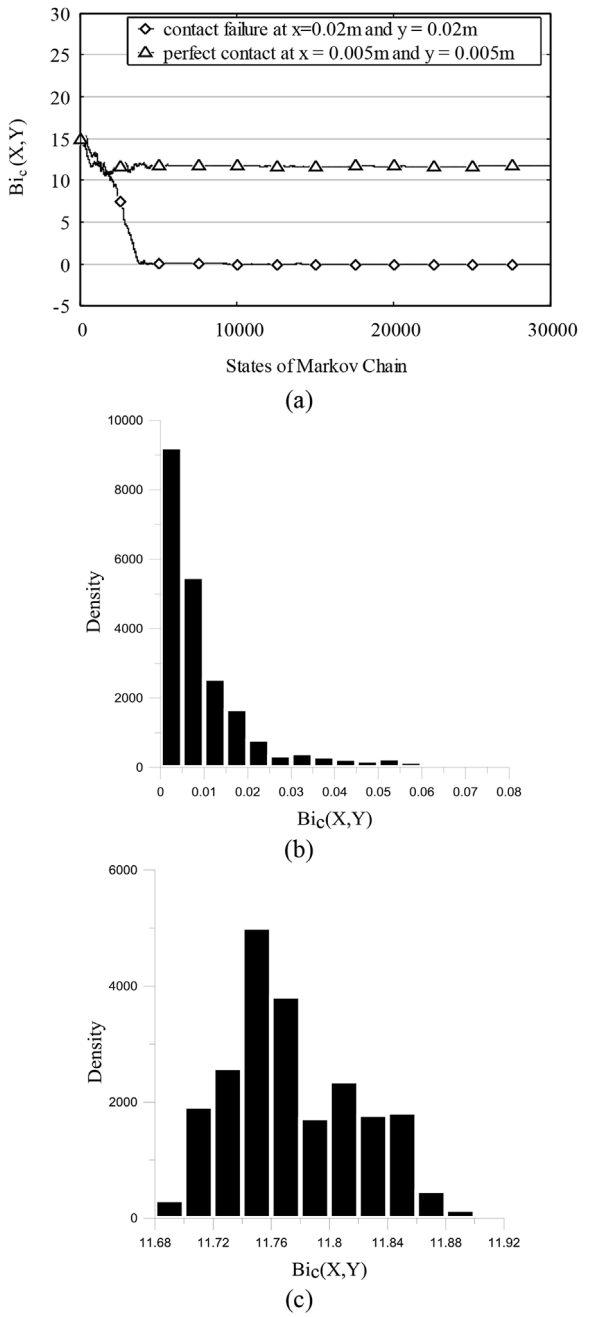

Fig. 12. (a) Markov chains of the estimated dimensionless contact conductance for the plate with circular failure obtained with 50 modes, (b) Histogram for a point of contact failure at $x = y = 0.02$ m, (c) Histogram for a point of perfect contact at $x = y = 0.005$ m.

provided by the MCMC samples.

The first mode of the transformed measurements is presented by Fig. 9a, while other selected modes are presented by Fig. 9b, for the plate with the circular contact failure. These figures show that the magnitude of the first mode was significantly larger than of the other modes and that the 50th mode was practically zero. Although not presented for the sake of brevity, such was also the case for the plate with a longitudinal failure. As a verification of the transformation process, the measured temperatures were then recovered by using 50 transformed modes through the application of the inverse formula given by equation (14.b). These temperatures are presented by Fig. 10a,b on a grid with 21 by 21 pixels, for the circular and longitudinal failures, respectively, at $t = 90$ s. A comparison of Figs. 8 and 10 reveals that the actual measurements and the temperatures recovered by using 50 modes are in excellent agreement, despite the fact that a reduced number of pixels was used for the results presented in Fig. 10. In fact, the temperatures recovered with the integral transformation/inversion were smoother than the actual measurements; hence, the measurement errors of high frequency in space and time were filtered out with the integral transformation and inversion based on the most important modes.

The estimation of the contact conductance $Bi_c(X,Y)$ in the plate with the circular failure, obtained with 50 modes, is presented by Fig. 11a,b.

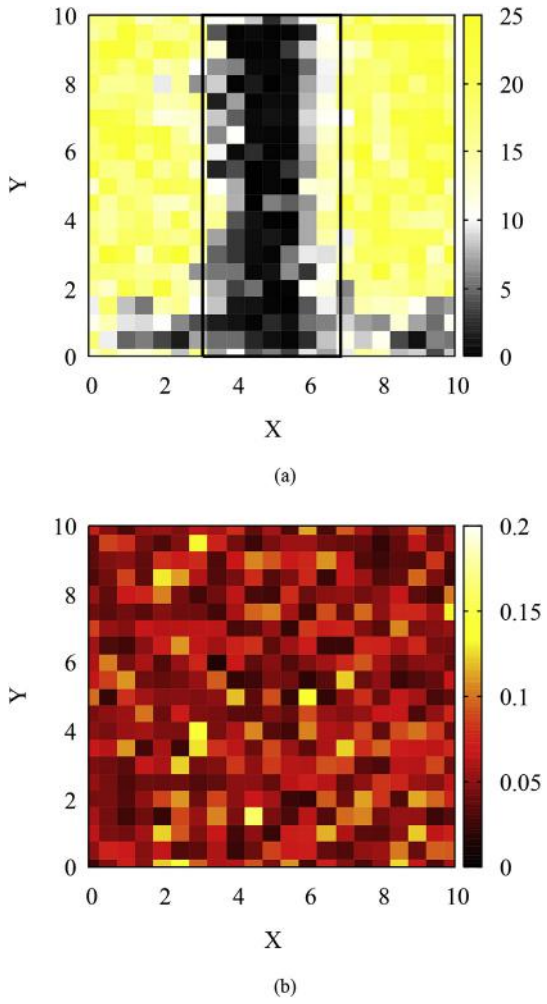

Fig. 13. Dimensionless contact conductance for the plate with longitudinal failure: (a) Estimated means obtained with 50 modes, (b) Estimated standard deviations obtained with 50 modes.

While Fig. 11a presents the means of the samples of the Markov chains after the burn-in period, Fig. 11b presents the standard deviations of these samples, for each pixel. Despite the non-informative prior and the small number of pixels used to recover this function, Fig. 11a,b shows that the position of the contact failure could be accurately detected with small uncertainties. Note that the contact conductance is approximately zero within the region of the contact failure and large in the region of perfect contact (see Fig. 11a), while the standard deviations are at least two order of magnitudes smaller that the estimated means of the contact conductance (see Fig. 11b). Hence, as for the case with simulated measurements, despite the fact that the measurements are compressed through the integral transformation in the spatial domain, the transformed modes are capable of retaining the information about the spatial variation of $Bi_c(X,Y)$. Furthermore, the estimated contact conductance is smooth and does not exhibit oscillations, even at the edge of the contact failure. Such a result reveals that the number of modes used for the likelihood function in the transformed domain (equation (16)) served as regularization of the inverse ill-posed problem, by filtering the high frequencies (noise) that would be amplified if more modes would be accounted for in the inverse analysis. Indeed, the solution of the inverse problem obtained with 200 modes was completely unstable, as shown by Fig. 11c. It should be noted that the non-informative uniform prior used here does not provide regularization, other than the non-negativity constraint, for the inverse problem solution. On the other hand, if the solution of the inverse problem is considered with the likelihood given by equation (13), Gaussian or Total Variation priors are required for appropriate regularization as shown in Refs. [3,4].

The Markov chains at a point of contact failure ($x = y = 0.02$ m) and at a point of perfect contact ($x = y = 0.005$ m) obtained with 50 modes in the plate with the circular failure, are shown by Fig. 12a. After starting at a condition of perfect contact, $Bi_c(X,Y) = 15$, the chains reached equilibrium in about 8000 states and converged towards 12 and 0 at the pixels of perfect contact and contact failure, respectively. The histograms of the samples of the Markov chains, between 10000 and 30000 states, at the pixels located at $x = y = 0.02$ m and $x = y = 0.005$ m are presented by Fig. 12b,c, respectively. Notice in Fig. 12b the skewed histogram at the point of contact failure, caused by the non-negativity constraint for $Bi_c(X,Y)$, represented by the prior given by equation (17). The histogram at the point of perfect contact presented by Fig. 12c shows that no samples were generated at regions of small $Bi_c(X,Y)$, at this point of perfect contact. Both histograms exhibit small posterior variances, as expected from the analysis of Fig. 11b.

Fig. 13a,b presents respectively the means and standard deviations of samples of the Markov chains, for the contact conductance $Bi_c(X,Y)$ at each pixel at the plate with the longitudinal failure, obtained with 50 modes. As for the circular failure, the longitudinal failure could be accurately detected with a small variance and the inverse problem solution was stable. Fig. 13a also shows that the contact between the plates was not perfect outside the manufactured failure for $Y < 2$ (the bottom of the image). The lack of attachment in this region was actually verified by a visual inspection of the target.

The temperature residuals (differences between measurements and temperatures calculated with the estimated parameters) are presented by Fig. 14a,b, for the plates with circular and longitudinal failures, respectively. These figures show the residuals at points of perfect contact ($x = 0.015$ m and $y = 0.01$ m) and contact failure ($x = y = 0.02$ m). The residuals are small, but correlated, despite the accurate predictions of the contact failures. Such behavior is due to the fact that the inverse problem was solved in the transformed temperature domain with a reduced number of modes and was also previously observed in cases involving one-dimensional data compression through integral transformation [17,44].

For the experiments with duration of 90s used in this work, the infrared camera provided 2,916,000 measurements. On the other hand, with the use of the likelihood function in the transformed domain with 50 modes, 40,500 transformed measurements were used in the inverse analysis, thus providing a data compression of 98.6%. In terms of computational time, the MCMC method with the likelihood function in the transformed domain with 50 modes took 3 h and 10 h, for the cases with the circular and longitudinal failures, respectively.

7. Conclusions

The detection of contact failures in layered composites was addressed in this work, by solving an inverse problem for the estimation of the contact conductance between the layers, with the Markov Chain Monte Carlo method. In addition to simulated data, actual temperature measurements obtained with an infrared camera over the surface of plates with two layers and controlled contact failures, were used in the inverse analysis. The estimation of the heat flux imposed by a radiant heater to the samples was also addressed in this work, by using both the MCMC method and the Kalman filter. The inverse problem of estimating the interface contact conductance was solved in a transformed domain, with measurements compressed by using the same integral transformation that was applied for the solution of the forward problem. The prior used for the unknown contact conductance was non-informative and only dealt with the fact that the contact conductance is non-negative. Circular and longitudinal failures were accurately detected with the proposed approach. Therefore, the transformed temperature modes were capable of appropriately retaining the information

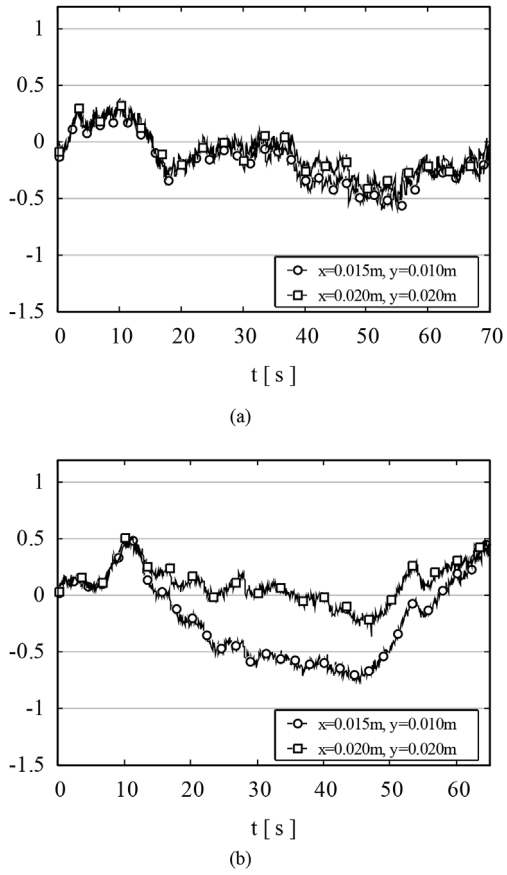

Fig. 14. Temperature residuals at selected points: (a) Plate with circular contact failure, (b) Plate with longitudinal contact failure.

about the spatial variation of the unknown function. It was also demonstrated that the use of the most significant transformed modes provided regularization for the inverse problem solution. Data compression was of at least 95%, which resulted in quite large speedups for the solution of the inverse problem.

Acknowledgments

The authors would like to thank the Brazilian agencies for the fostering of science, *Conselho Nacional de Desenvolvimento Científico e Tecnológico* (CNPq) (304936-2014-6), *Coordenação de Aperfeiçoamento de Pessoal de Nível Superior* (CAPES) and *Fundação Carlos Chagas Filho de Amparo à Pesquisa do Estado do Rio de Janeiro* (FAPERJ) (203725), as well as the Academy of Finland (Center of Excellence in Inverse Modelling and Imaging, project 312343), for the financial support for this work. The samples with controlled faults were kindly manufactured by Dr. José Martim in LabMems/COPPE/UFRJ.

References

[1] D. Gay, Composite Materials: Design and Applications, third ed., CRC Press, Taylor & Francis, Boca Raton, 2015.
[2] C. Meola, G.M. Carlomagno, Recent advances in the use of infrared thermography, Meas. Sci. Technol. 15 (2004) R27.
[3] L.A.S. Abreu, H.R.B. Orlande, C.P. Naveira-Cotta, J.N.N. Quaresma, R.M. Cotta, J. Kaipio, V. Kolehmainen, Identification of contact failures in multi-layered composites, ASME 2011 International Design Engineering Technical Conference and Computers and Information in Engineering Conference, Washington, DC, USA, 2011, pp. 479–487.
[4] L.A.S. Abreu, H.R.B. Orlande, J. Kaipio, V. Kolehmainen, R.M. Cotta, J.N.N. Quaresma, Identification of contact failures in multilayered composites with the Markov chain Monte Carlo method, J. Heat Transfer 136 (2014) 101302.
[5] L.A.S. Abreu, M.J. Colaço, C.J.S. Alves, H.R.B. Orlande, V. Kolehmainen, J. Kaipio, A comparison of two inverse problem techniques for the identification of contact failures in multi-layered composites, 22nd International Congress of Mechanical Engineering (COBEM 2013), Ribeirão Preto, Brazil, 2013, pp. 5422–5432.
[6] L.A.S. Abreu, H.R.B. Orlande, M.J. Colaço, C.J.S. Alves, Detection of contact failures in laminated composites by infrared thermography: description of the experimental apparatus and initial results, 15th Brazilian Congress of Thermal Sciences and Engineering (ENCIT2014), Belém, PA, Brazil, 2014.
[7] L.A.S. Abreu, C.J.S. Alves, M.J. Colaço, H.R.B. Orlande, A non-intrusive inverse problem technique for the identification of contact failures in double-layered composites, Proc. of 15th International Heat Transfer Conference, Kyoto, Japan, 2014.
[8] L.A.S. Abreu, M.J. Colaço, H.R.B. Orlande, C.J.S. Alves, Detection of contact failures, 6th International Conference on Mechanics and Materials in Design, 2015, Ponta Delgada/Azores, 2015.
[9] L.A.S. Abreu, M.J. Colaço, H.R.B. Orlande, C.J.S. Alves, Thermography detection of contact failures in double layered materials using the reciprocity functional approach, Appl. Therm. Eng. 100 (2016) 1173–1178.
[10] R.S. Padilha, M.J. Colaço, H.R.B. Orlande, L.A.S. Abreu, An analytical method to estimate spatially-varying thermal contact conductances using the reciprocity functional and the integral transform methods: theory and experimental validation, Int. J. Heat Mass Tran. 100 (2016) 599–607.
[11] M.J. Colaço, C.J.S. Alves, A backward reciprocity function approach to the estimation of spatial and transient thermal contact conductance in double-layered materials using non-intrusive measurements, Numer. Heat Tran., Part a: Applications 68 (2) (2015) 117–132.
[12] M.J. Colaço, C.J.S. Alves, H.R.B. Orlande, Transient non-intrusive method for estimating spatial thermal contact conductance by means of the reciprocity functional approach and the method of fundamental solutions, Inverse Problems in Science and Engineering 23 (4) (2015) 688–717.
[13] M. Grosso, C.A. Marinho, D.A. Nesteruk, J.M. Rebello, S.D. Soares, V.P. Vavilov, Evaluating quality of adhesive joints in glass-fiber plastic piping by using active thermal NDT, Proc. SPIE 8705, Thermosense: Thermal Infrared Applications XXXV, Baltimore, Maryland, USA, 2013, p. 87050T.
[14] M. Grosso, J.E.C. Lopez, V.M.A. Silva, S.D. Soares, J.M.A. Rebello, G.R. Pereira, Pulsed thermography inspection of adhesive composite joints: computational simulation model and experimental validation, Compos. B Eng. 106 (2016) 1–9.
[15] A.N. Smith, N.R. Jankowski, L.M. Boteler, Measurement of high-performance thermal interfaces using a reduced scale steady-state tester and infrared microscopy, J. Heat Tran. 138 (2016) 041301.
[16] C.P. Naveira-Cotta, R.M. Cotta, H.R.B. Orlande, Inverse analysis with integral transformed temperature fields: identification of thermophysical properties in heterogeneous media, Int. J. Heat Mass Tran. 54 (2011) 1506–1519.
[17] D. Knupp, C. Naveira-Cotta, J. Ayres, H. Orlande, R. Cotta, Space-variable thermophysical properties identification in nanocomposites via integral transforms, Bayesian inference and infrared thermography, Inverse Prob. Sci. Eng. (2012) 1–29.
[18] D.C. Knupp, L.A.S. Abreu, Explicit boundary heat flux reconstruction employing temperature measurements regularized via truncated eigenfunction expansions, Int. Commun. Heat Mass Tran. 78 (2016) 241–252.
[19] E.P. Barrio, J.L. del, Dauvergne, Karhunen-loeve Decomposition for Data, Noise, and Model Reduction in Inverse Problems, Chapter 14 in *Thermal Measurements and Inverse Techniques*, in: H. Orlande, O. Fudym, D. Maillet, R. Cotta (Eds.), CRC Press, 2011.
[20] R.A. Bialecki, A.J. Kassab, A. Fic, Proper orthogonal decomposition and modal analysis for acceleration of transient FEM thermal analysis, Int. J. Numer. Meth. Eng. 62 (2005) 774–797.
[21] R.A. Białecki, A.J. Kassab, Z. Ostrowski, Application of the proper orthogonal decomposition in steady state inverse problems, Inverse Problems in Engineering Mechanics IV, Elsevier, 2003, pp. 3–12.
[22] A. Fic, R.A. Białecki, A.J. Kassab, Solving transient nonlinear heat conduction problems by proper orthogonal decomposition and the finite-element method, Numer. Heat Tran., Part B: Fundamentals 48 (2005) 103–124.
[23] Z. Ostrowski, Application of Proper Orthogonal Decomposition to the Solution of Inverse Problems, Silesian University of Technology, Gliwice, Poland, 2006.
[24] Z. Ostrowski, R.A. Bialecki, A. Fic, POD-rbf network approximation for inverse problem solutions, Proceedings of Inverse Problems, Design and Optimization Symposium (IPDO-2007), Miami, Florida, 2007, pp. 295–300.
[25] J. Berger, H.R.B. Orlande, N. Mendes, Proper Generalized Decomposition model reduction in the Bayesian framework for solving inverse heat transfer problems, Inverse Problems in Science and Engineering 25 (2) (2017) 260–278.
[26] M.N. Ozisik, Heat Conduction, McGraw Hill, New York, 1993.
[27] R.M. Cotta, Hybrid numerical-analytical approach to nonlinear diffusion problems, Numer. Heat Tran., Part B- Fundamentals 127 (1990) 217–226.
[28] R.M. Cotta, Integral Transforms in Computational Heat and Fluid Flow, CRC Press, Boca Raton, Florida, 1993.
[29] R.M. Cotta, Benchmark results in computational heat and fluid flow: - the integral transform method, Int. J. Heat Mass Tran. 37 (1) (1984) 381–394.
[30] R.M. Cotta, M.D. Mikhailov, Heat Conduction: Lumped Analysis, Integral Transforms, Symbolic Computation, Wiley-Interscience, New York, 1997.
[31] R.M. Cotta, The Integral Transform Method in Thermal and Fluids Sciences and Engineering, Begell House, New York, 1998.
[32] R. Cotta, M. Mikhailov, Hybrid methods and symbolic computations, in: W.J. Minkowycz, E.M. Sparrow, J.Y. Murthy (Eds.), Handbook of Numerical Heat Transfer, second ed., John Wiley, New York, 2006, pp. 493–522 Chapter 16.
[33] E.J. Corrêa, R.M. Cotta, H.R.B. Orlande, On the reduction of computational costs in eigenfunction expansions of multidimensional diffusion problems, Int. J. Numer. Meth. Heat Fluid Flow 7 (1997) 675–695.
[34] M.N. Özisik, H.R.B. Orlande, M.J. Colaço, R.M. Cotta, Finite Difference Methods in

Heat Transfer, second ed., CRC Press, Boca Raton, 2017.
[35] J. Kaipio, E. Somersalo, Statistical and Computational Inverse Problems, Applied Mathematical Sciences 160, Springer-Verlag, 2004.
[36] S. Tan, C. Fox, G. Nicholls, Inverse Problems, Course Notes for Physics 707, University of Auckland, 2006.
[37] H. Orlande, F. Fudym, D. Maillet, R. Cotta, Thermal Measurements and Inverse Techniques, CRC Press, Boca Raton, 2011.
[38] D. Gamerman, H.F. Lopes, Markov Chain Monte Carlo: Stochastic Simulation for Bayesian Inference, second ed., Taylor & Francis, Boca Raton, 2006.
[39] H.R.B. Orlande, V. Kolehmainen, J.P. Kaipio, Reconstruction of thermal parameters using a tomographic approach, Int. J. Heat Mass Tran. 50 (2007) 5150–5160.
[40] A.F. Emery, Estimating deterministic parameters by bayesian inference with emphasis on estimating the uncertainty of the parameters, Proceedings of the Inverse Problem, Design and Optimization Symposium, vol. I, 2007, pp. 266–272 (Miami Beach, Florida).
[41] C. Mota, H. Orlande, M. De Carvalho, V. Kolehmainen, J. Kaipio, Bayesian estimation of temperature-dependent thermophysical properties and transient boundary heat flux, Heat Tran. Eng. 31 (2010) 570–580.
[42] C. Naveira-Cotta, H. Orlande, R. Cotta, Integral transforms and bayesian inference in the identification of variable thermal conductivity in two-phase dispersed systems, Numer. Heat Tran. Part B, Fundamentals 57 (2010) 173–202.
[43] C. Naveira-Cotta, R. Cotta, H. Orlande, Inverse analysis of forced convection in micro-channels with slip flow via integral transforms and Bayesian inference, Int. J. Therm. Sci. 49 (2010) 879–888.
[44] H. Massard, O. Fudym, H.R.B. Orlande, F. Sepulveda, A statistical inversion approach for local thermal diffusivity and heat flux simultaneous estimation, Quant. InfraRed Therm. J. 11 (2014) 170–189.
[45] H. Orlande, M. Colaço, G. Dulikravich, Approximation of the likelihood function in the Bayesian technique for the solution of inverse problems, Inv. Prob. Sci. Eng. 16 (2008) 677–692.
[46] J. Kaipio, C. Fox, The bayesian framework for inverse problems in heat transfer, Heat Tran. Eng. 32 (2011) 718–753.
[47] A. Nissinen, L. Heikkinen, J. Kapio, The Bayesian approximation error approach for electrical impedance tomography – experimental results, Meas. Sci. Technol. 19 (2008), http://dx.doi.org/10.1088/0957-0233/19/1/015501.
[48] A. Nissinen, L. Heikkinen, V. Kolehmainen, J. Kapio, Compensation of errors due to the discretization, domain truncation and unknown contact impedances in electrical impedance tomography, Meas. Sci. Technol. 20 (2009).
[49] A. Nissinen, V. Kolehmainen, J. Kapio, Compensation of modeling errors due to the unknown domain boundary in electrical impedance tomography, IEEE Trans. Med. Imag. 30 (2011) 231–242.
[50] V. Kolehmainen, T. Tarvainen, S.R. Arridge, J.P. Kaipio, Marginalization of uninteresting distributed parameters in inverse problems – application to diffuse optical tomography, Int. J. Uncertain. Quantification 1 (2011) 1–17.
[51] C.C. Pacheco, H.R.B. Orlande, M.J. Colaço, G.S. Dulikravich, Estimation of a location- and time-dependent high-magnitude heat flux in a heat conduction problem using the kalman filter and the approximation error model, Numer. Heat Tran., Part a: Applications 68 (2015) 1198–1219.
[52] C.C. Pacheco, H.R.B. Orlande, M.J. Colaço, G.S. Dulikravich, Real-time identification of a high-magnitude boundary heat flux on a plate, Inv. Prob. Sci. Eng. 24 (9) (2016) 1661–1679.
[53] J.A. Christen, C. Fox, Markov chain Monte Carlo using an approximation, J. Comput. Graph Stat. 14 (2005) 795–810.
[54] T. Cui, C. Fox, M.J. O'Sullivan, Bayesian calibration of a large-scale geothermal reservoir model by a new adaptive delayed acceptance Metropolis Hastings algorithm, Water Resour. Res. 47 (2011) W10521.
[55] W.D. Callister, D.G. Rethwisch, Materials Science and Engineering: an Introduction, Wiley New York, 2007.